

DENDRITIC STRUCTURE VARIES AS A FUNCTION OF ECCENTRICITY IN V1: A QUANTITATIVE STUDY OF NADPH DIAPHORASE NEURONS IN THE DIURNAL SOUTH AMERICAN RODENT AGOUTI, *DASYPROCTA PRYMNOLOPHA*

E. G. DA ROCHA,^{a†} M. A. M. FREIRE,^{a,b†} C. P. BAHIA,^a A. PEREIRA,^c M. C. K. SOSTHENES,^a L. C. L. SILVEIRA,^d G. N. ELSTON^e AND C. W. PICANÇO-DINIZ^{a*}

^aLaboratory of Investigations in Neurodegeneration and Infection, Federal University of Pará, Hospital Universitário João de Barros Barreto, Rua dos Mundurucus 4487, 66073-000 Belém/PA, Brazil

^bEdmond and Lily Safra International Institute of Neurosciences of Natal, Rua Prof. Francisco Luciano de Oliveira 2460, 59066-060 Natal/RN, Brazil

^cBrain Institute, Federal University of Rio Grande do Norte, Av. Nascimento de Castro 2155, 59056-450 Natal/RN, Brazil

^dLaboratory of Neurophysiology Professor Eduardo Oswaldo-Cruz, Institute of Biological Sciences, Federal University of Pará, 66075-990 Belém/PA, Brazil

^eCentre for Cognitive Neuroscience, Sunshine Coast, Queensland 4562, Australia

Abstract—The cerebral cortex is often described as a composite of repeated units or columns, integrating the same basic circuit. The ‘ice-cube’ model of cortical organization, and ‘canonical’ circuit, born from insights into functional architecture, still require systematic comparative data. Here we probed the anatomy of an individual neuronal type within V1 to determine whether or not its dendritic trees are consistent with the ‘ice-cube’ model and theories of canonical circuits. In a previous report we studied the morphometric variability of NADPH-diaphorase (NADPH-d) neurons in the rat auditory, visual and somatosensory primary cortical areas. Our results suggested that the nitroergic cortical circuitry of primary sensory areas are differentially specialized, probably reflecting peculiarities of both habit and behavior of the species. In the present report we specifically quantified the dendritic trees of NADPH-d type I neurons as a function of eccentricity within V1. Individual neurons were reconstructed in 3D, and the size, branching and space-filling of their dendritic trees were correlated with their location within the visuotopic map. We found that NADPH-d neurons became progressively smaller and less branched with progression from the central visual representation to the intermediate and peripheral visual representation. This finding suggests that aspects of cortical circuitry may vary across the cortical mantle to a greater extent than envisaged

as natural variation among columns in the ‘ice-cube’ model. The systematic variation in neuronal structure as a function of eccentricity warrants further investigation to probe the general applicability of columnar models of cortical organization and canonical circuits. © 2012 IBRO. Published by Elsevier Ltd. All rights reserved.

Key words: agouti, area 17, cutia, striate cortex, visual streak.

INTRODUCTION

The organization of the cerebral cortex has been the focus of considerable investigation since techniques allowed the visualization of microscopic circuitry. Over the past 50 years or so much attention has been focused on the study of the functional organization of cortex. Hubel and Wiesel, in a series of defining studies (Hubel and Wiesel, 1974, 1977), suggested that ocular dominance columns in the macaque monkey striate cortex might be bands of uniform width that intersect orthogonally and that the extended concept of cortical column is what they termed ‘hypercolumns’, a complete array of columns that analyzes all values of a given variable, for review see Ts'o et al. (2009). Together with earlier findings of Vernon Mountcastle describing the cortical column in somatosensory cortex these ideas supported a modular view of the organization of neocortex (Mountcastle, 1957, 1997). Hubel and Wiesel developed their ‘ice-cube’ model of cortical organization (Hubel and Wiesel, 1977), which is commonly reproduced in texts. This model, based on electrophysiological recording, posits that the cortical mantle is composed of repeated units of similar function uniformly distributed in V1 visual field representation; see Ts'o et al. (2009) for review. In addition the architectonic similarities of laminar circuitry in different neocortical regions were associated with the idea of a canonical local circuit for the neocortex; see Douglas and Martin (2007) for review. However it has been difficult to determine whether or not these models of neocortical organization are applied to the inhibitory neocortical circuits and a series of anatomical data suggest diversity rather than uniformity between regions and cells, possibly associated with functional specializations, see Elston (2007) and Katzel et al. (2011) for review. For example, differences have been revealed the structural organization of inhibitory neurons such as chandelier cells, double bouquet cells, bipolar cells and

*Corresponding author. Tel: +55-91-3201-6757.

E-mail addresses: cwpdiniz@gmail.com, cwpdiniz@ufpa.br (C.W. Picanço-Diniz).

† E. G. da Rocha and M. A. M. Freire contributed equally to the work. **Abbreviations:** NADPH-d, nicotinamide adenine dinucleotide phosphate; PMBSF, posterior medial barrel subfield; ALBSF, anterolateral medial barrel subfield.

their connections among cortical areas (Kritzer et al., 1992; Conde et al., 1996; Defelipe et al., 1999). In addition, it has been described that pyramidal cells, (the major neuronal component of the cerebral cortex), sample different proportions of barrels in the posterior medial barrel subfield (PMBSF) and anterolateral medial barrel subfield (ALBSF) in the primary somatosensory area (S1) of the rat (Elston et al., 1997) and different numbers of inhibitory neurons are located within the dendritic trees of cells in the two different barrel subfields (Elston et al., 1999a). The dendritic trees of pyramidal cells located in the interblobs in monkey V1 are smaller than those in the blobs (Elston and Rosa, 1998) and the density of neurons has been shown to differ between these two regions (Collins et al., 2010). There are also systematic differences in the size and branching complexity of the dendritic trees of pyramidal cells, and their intrinsic horizontal projections, among cortical areas; with a serial increase in the size of the dendritic trees of pyramidal cells and their intrinsic axon patches through visual areas of the ‘what’ and ‘where’ pathways (Lund et al., 1993; Fujita and Fujita, 1996; Elston and Rosa, 1997, 1998; Elston et al., 1999a,b).

In a previous report we collected morphometric data of NADPH-diaphorase (NADPH-d) neurons in primary auditory, visual and somatosensory rat cortices (Freire et al., 2012). This analysis of NADPH-d neurons allowed us to distinguish three groups of cells, corresponding to the three analyzed areas. S1 neurons have a higher morphological complexity than those found in both A1 and V1.

In the present study we add another piece of evidence to these data that is not consistent with the concept of repeating unit architecture in the striate cortex. We investigated the morphology of NADPH-d type I neurons along the naso-temporal axis in V1 at the visual streak representation to seek systematic differences in the number, size and branching complexity of their dendritic trees. These neurons comprise a sub-population of inhibitory interneurons (Vincent and Kimura, 1992), including those that form long distance inhibitory projections (Higo et al., 2007). We found that the dendritic trees of NADPH-d type I neurons were larger and more branched in the central visuotopic representation as compared with those in the peripheral visuotopic representation. Moreover, we found a higher density of NADPH-d neurons in the central representation, as compared with the peripheral representation. We have chosen for the present study the South American rodent *Dasyprocta primnolopha*, also known as the agouti. Fully grown male agoutis weight between 2.0 and 3.5 kg, have a large lissencephalic brain, which is well suited for mapping studies (Picanco-Diniz et al., 1991) as compared with smaller rodents such as rat (Espinoza and Thomas, 1983) and mouse (Wagor et al., 1980). The agouti is a highly visual rodent with prominent visual streak in the retina (Silveira et al., 1989) and an asymmetric representation of the horizon in V1 as described previously in many lateral-eyed mammals (Picanco-Diniz et al., 1992) providing an excellent opportunity for comparative studies of cortical organization (Rocha et al., 2007; Santiago et al., 2007).

EXPERIMENTAL PROCEDURES

Animals

Tissue was obtained from captive-bred animals used in other electrophysiological experiments (Picanco-Diniz et al., 2011). Data for the present study were obtained from five adult male agoutis (*Dasyprocta primnolopha*), weighing between 2.6 and 3.2 kg (Table 1), sourced from the Museu Paraense Emilio Góeldi animal colony. The use of agoutis for scientific experimentation was in accordance with guidelines from the Brazilian Institute of the Environment and Renewable Natural Resources (IBAMA) (license 207419-0030/2003). All experimental procedures were carried out strictly in accordance with the National Institute of Health Guide for the Care and Use of Laboratory Animals (NIH Publications No. 80-23), under license of the Ethics Committee on Experimental Animals of the UFPA.

Perfusion, tissue preparation and histochemical processing

Animals were deeply anaesthetized with either urethane (1.25 mg/kg, *i.p.*) or a mixture of ketamine chloridrate (10 mg/kg) and xylazine chloridrate (1 mg/kg, *i.p.*) and perfused transcardially with 0.9% heparinized-saline, followed by 4% paraformaldehyde (Sigma Company, St Louis, MO, USA) in 0.1 M phosphate buffer (PB), pH 7.4. The brains were removed from the skull, sectioned coronally at 250 μ m in a vibratome (Pelco International, Series 1000, Ted Pella Inc., Redding, CA, USA) and processed for NADPH-d histochemistry (Scherer-Singler et al., 1983). In brief, the sections were incubated in a solution containing 0.6% malic acid, 0.03% nitroblue tetrazolium, 1% dimethylsulfoxide, 0.03% manganese chloride, 0.5% β -NADP and 1.5–3% Triton X-100 in 0.1 M Tris buffer, pH 8.0. The reaction was monitored every 30 min to avoid overstaining and was interrupted by rinsing the sections in Tris buffer (pH 8.0). Usually all histochemical reactions ended in no more than 2 h. Sections were then mounted onto gelatinized-glass slides, air-dried overnight, dehydrated through a series of graded alcohols and coverslipped with Entellan (Merck, Germany). Another set of animals were perfused, cut at 70 μ m thick and stained for Nissl substance and patterns of myelination (Gallyas, 1979).

From another set of animals serial sections were cut from flat-mount preparations, including the entire exposed portion of V1 see Elston et al. (2006) for details. Even in the unstained tangential sections it is possible to identify that which contains layer IV due to its ‘milky’ color, and its position within all sections from the pial surface to white matter. Layer IV was also identified by processing the sections for Nissl substance, being characterized by relatively closely spaced small cell bodies of granular cells as opposed to the larger less densely spaced pyramidal cells of adjacent layers. Only neurons with their cell body located in

Table 1. Summary of the animals utilized

Animal	Age (months)	Body weight (kg)	Brain weight (g)
Dp_V1-01	18	2.9	17.2
Dp_V1-02	21	2.6	15.9
Dp_V1-03	19	3.2	17.6
Dp_V1-04	20	2.7	16.3
Dp_V1-05	18	3.2	17.1

Similar number of cells for three-dimensional reconstructions were taken from each region of interest of each animal.

layers II and III, as identified as being supra-adjacent to granular layer IV, were included for analysis. Only cells that were fully impregnated and had their complete dendritic tree contained within a single section (250 μm thick) were included for analyses.

Electrode penetrations resulting from previous electrophysiological studies in which we mapped the functional topography in V1 were correlated with anatomical landmarks by reconstructing across a series of sections. A composite map of V1 topography was constructed from electrophysiological data obtained in the previous mapping studies, to assist in the present study, see Fig. 2 of Picanço-Diniz et al. (2011). A digitizing table was then used to measure the lateral position of each penetration in relation to the fundus of the lateral sulcus by generating a flat map reconstruction of the visual recording sites; see Figs. 1B and 4 from Picanço-Diniz et al. (1991).

Neuronal reconstruction and quantitative analysis

A total of 120 NADPH-d type I neurons were reconstructed in 3D with aid of an Optiphot-2 microscope (Nikon, Tokyo, Japan) equipped with an oil immersion, 60 \times plan apochromatic objective lens, a motorized stage (MAC200, LUDL, Hawthorne, NY, USA) and a computer running the *NeuroLucida* software (MBF Bioscience Inc., Frederick, MD, USA). For the purpose of the present investigation, we included only NADPH-d type I neurons. As previously mentioned, only cells with a dendritic tree unequivocally complete were included for analysis (cells whose dendrites seemed to be artificially cut or apparently not fully impregnated were discarded). Terminal dendrites were typically thin, presenting a round tip. The cells (40 for each cortical area, 24 from each animal) were selected from three different regions along the visual streak representation as follows: near the vertical meridian (lateral region, $n = 8 \times 5$), near the optical axis (68° eccentricity – intermediate region, $n = 8 \times 5$) and at the far temporal periphery ($n = 8 \times 5$) near the lateral sulcus (beyond 140° eccentricity – medial region). In these chosen sections the lateral margin of V1 was clearly depicted by neuropil changes of NADPH-d reacted sections that becomes darker at layer IV just in the limit with V2 (where the vertical meridian is represented) whereas the medial margin of V1 was localized at the bottom of the medial bank of lateral sulcus. Six parameters were evaluated: (1) cell body size; (2) size of dendritic tree (defined by the polygon joining the outermost distal tips of the dendrites); (3) number of dendrites by order; (4) dendritic branching (Faro et al., 1995); (5) fractal dimension (D) – including both the dilatation and mass radius methods (Jelinek and Fernandez, 1998); and (6) convex hull analysis. Convex hull was defined as a connected series of straight segments convexly enclosing all of the cell branches to decide whether cell populations from different cortical areas could be distinguished on the basis of shape (Pincus and Theriot, 2007). The size of the cell body, the size of the dendritic tree and the number of branches (by order) were determined with the aid of *Neuroexplorer* software (MBF Bioscience Inc., USA). By focusing through the depth of the cell body it is relatively easy to distinguish the cell body from the dendrites issuing from the cell body by changes in the contours. In this way we determined the size of the cell bodies. The size of the dendritic tree was determined as that included in a convex polygon joining the outermost distal tips of the dendrites in 2D tangential images of the 3D reconstruction of each neuron (e.g., Elston et al., 2006b). The number of dendrites by order was determined by tracing the individual dendrites and relying on features of *Neuroexplorer* to rank the order of each segment of dendrite and quantify them. The fractal dimension and convex hull analyses were performed with the *Scion Image* software (Scion Corporation, Frederick, MD, USA). In addition, we performed a cluster analysis in our sample using data obtained for the size of dendritic tree, cell body size, number of dendrites by order, convex hull factor, and fractal dimension as parameters

(Schweitzer and Renehan, 1997). The resulting group distribution was further evaluated by a forward stepwise discriminant function analysis using the software Statistica 6.0 (StatSoft Inc., Tulsa, OK, USA), in order to determine which variables better discriminated those groups.

Determination of the density of NADPH-d neurons

The density of NADPH-d-stained neurons was determined by bi-dimensional reconstruction of the flat mounted cortical sections. We delineated the regions of interest by placing bi-dimensional counting probes of equal areas inside each region using the lateral sulcus and the electrophysiological map of V1 as reference points. Cells were counted with the aid of a low resolution, 3.2 \times objective coupled with an Optiphot-2 microscope (Nikon, Tokyo, Japan), equipped with a motorized stage (MAC200, Ludl Electronic Products, Hawthorne, NY, USA). Because type I NADPH-d cells are relatively sparse it was simple to count them all in the whole set of sections containing the areas of interest. For that reason cell counts represent the total number of type I cell in the counting probes. To do so NADPH-d cell bodies that came into focus inside the counting frame were counted and added to the total number of markers, provided their cell bodies were entirely within the counting frame or intersected the acceptance lines without touching the rejection lines. NADPH-d-stained cellular fragments cut at the level of a dendritic tree, or ambiguously labeled cell bodies were not included. To estimate the cell densities we divided the total number of cells by the fixed area of the counting probe (cells/mm²). The cell densities were quantified in the central, intermediate and peripheral visual representation (Fig. 1.).

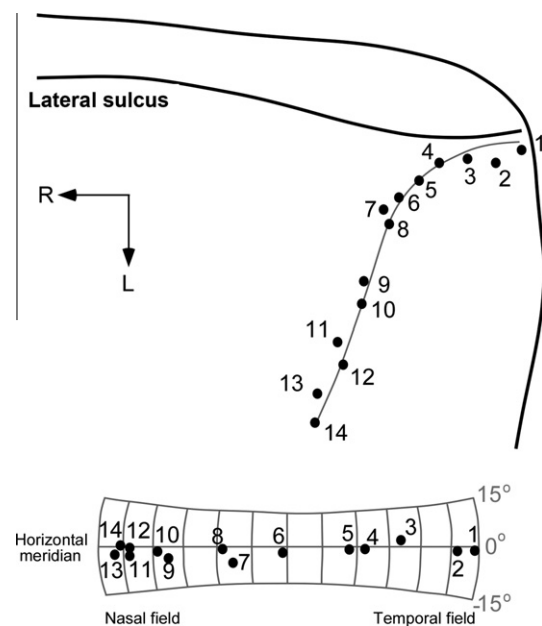


Fig. 1. Graphic representation of individual recording sites of neurons in the primary visual cortex of the agouti (top) and the relative location of their receptive fields in visuotopic space (bottom). Note in V1 the nasal representation is located laterally and the peripheral representation is located medially, adjacent to the lateral sulcus. Solid circles indicate the center of the receptive fields on equatorial/azimuthal map of the visual field, and the equivalent cortical recording sites aligned with the representation of the horizontal meridian in V1. Numbers indicate cortical recording sites and equivalent receptive field centers. Legends: R: rostral, L: lateral.

Statistical analysis

Data obtained from estimation of cell number and morphometric analysis of cells sampled from the central, intermediate and peripheral visual representation were tested by analysis of variance (ANOVA). Pairwise *post hoc* tests were performed with the Newman–Keuls test. The significance level was set at 95% ($p < 0.05$) for all comparisons.

Photomicrographic documentation and processing

To obtain digital photomicrographs, we used a digital camera (Microfire, Optronics, CA, USA) coupled to a Nikon microscope (Optiphot-2, Tokyo, Japan). Digital photomicrographs were processed using Adobe Photoshop CS (Adobe Systems Inc., San José, CA, USA) for scaling and adjusting the levels of brightness and contrast. Selected pictures in the figures were taken from

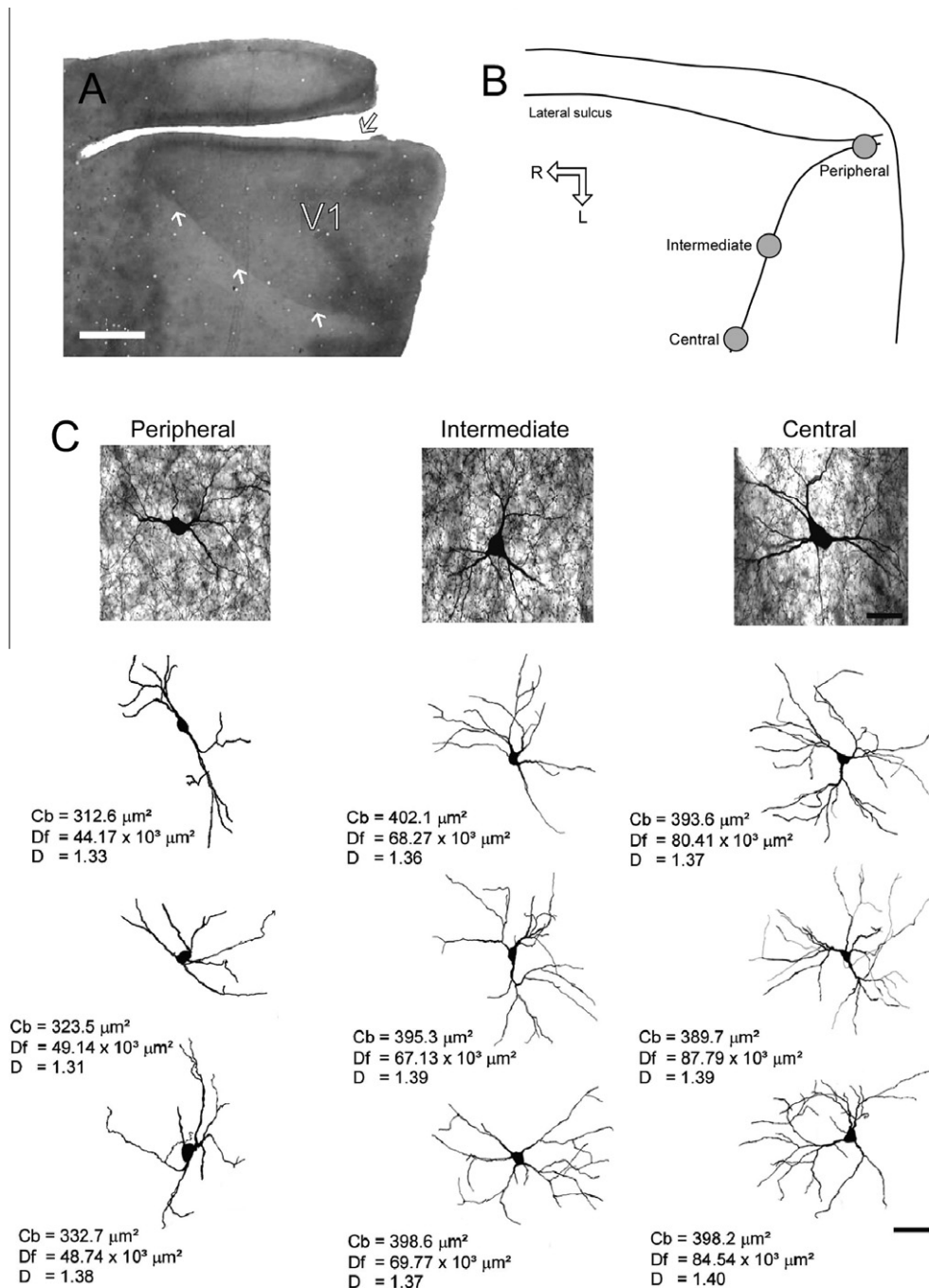


Fig. 2. Photomicrograph of a flat mount of the agouti brain that was processed for NADPH-d histochemistry to illustrate V1 area (A), adjacent to and extending underneath the lateral sulcus (large arrow), and a schematic drawing of the regions of interest (B). The smaller arrows and the larger one in (A) point to the lateral and medial borders of V1, respectively. Photomicrographs of examples of NADPH-d type I cells located in the peripheral, intermediate and central visuotopic representation that were included for analysis (C). Individual neurons were reconstructed and aspects of their morphology quantified, revealing differences in the size and branching structure of their dendritic trees (bottom of C). Legends: Cb: cell body; Df: dendritic field; D: fractal dimension (dilation method). R: rostral, L: lateral. Scale bars = 2 mm (A, B); 50 μm (C, top); 100 μm (C, bottom).

sections of the subjects of each experimental group with objects of interest nearest the mean value of each region of interest.

RESULTS

Analysis of NADPH-d type I neurons according to their topographic location within V1

Differences in the intensity of labeling within sections processed for NADPH-d made it possible to unambiguously identify the extent of V1 (Fig. 2A), consistent with previous cytoarchitectonic, myeloarchitectonic, histochemical and electrophysiological mapping studies (Picanço Diniz et al., 1989; Elston et al., 2006; Freire et al., 2010). Note that the lateral and medial limits of V1 are conspicuously defined (arrows in Fig. 2A) and are consistent with previous findings based on gross location of this sulcus. Fig. 2B is a schematic representation of V1 to illustrate relative locations from where neurons were sampled in the present investigation.

NADPH-d stained coronal sections across V1 revealed a clear laminar pattern where supragranular layers as compared to infragranular layers, showed a

darker staining that co-localizes with layers II and III in Nissl staining. The entire V1 area is permeated by a network of fine varicose NADPH-d stained fibers, which branched extensively throughout the tissue, as well as by a diffuse blue pattern in the neuropil in all layers. The histochemical reaction also revealed two different types of NADPH-d stained cells: a slightly stained subpopulation (type II) and a subgroup of deeply stained neurons resembling a Golgi impregnation (type I). These type I cells were nonpyramidal neurons typically smooth or very sparsely spiny. Their dendritic arbors were very well stained but their axons were not always evident (Fig. 2C). These heavily stained neurons showed variable dendritic tree morphologies and, based on these morphologies, are likely to be defined as local circuit neurons (Gabbott and Bacon, 1995; Luth et al., 1994).

The size of the cell bodies of NADPH-d type I neurons in the intermediate ($396.5 \pm 21.02 \mu\text{m}^2$) and central ($393.78 \pm 23.53 \mu\text{m}^2$) visuotopic representations were larger than those in the peripheral representation ($351.47 \pm 18.25 \mu\text{m}^2$; mean \pm SEM) (Fig. 3A). An analysis of variance revealed these differences to be significant

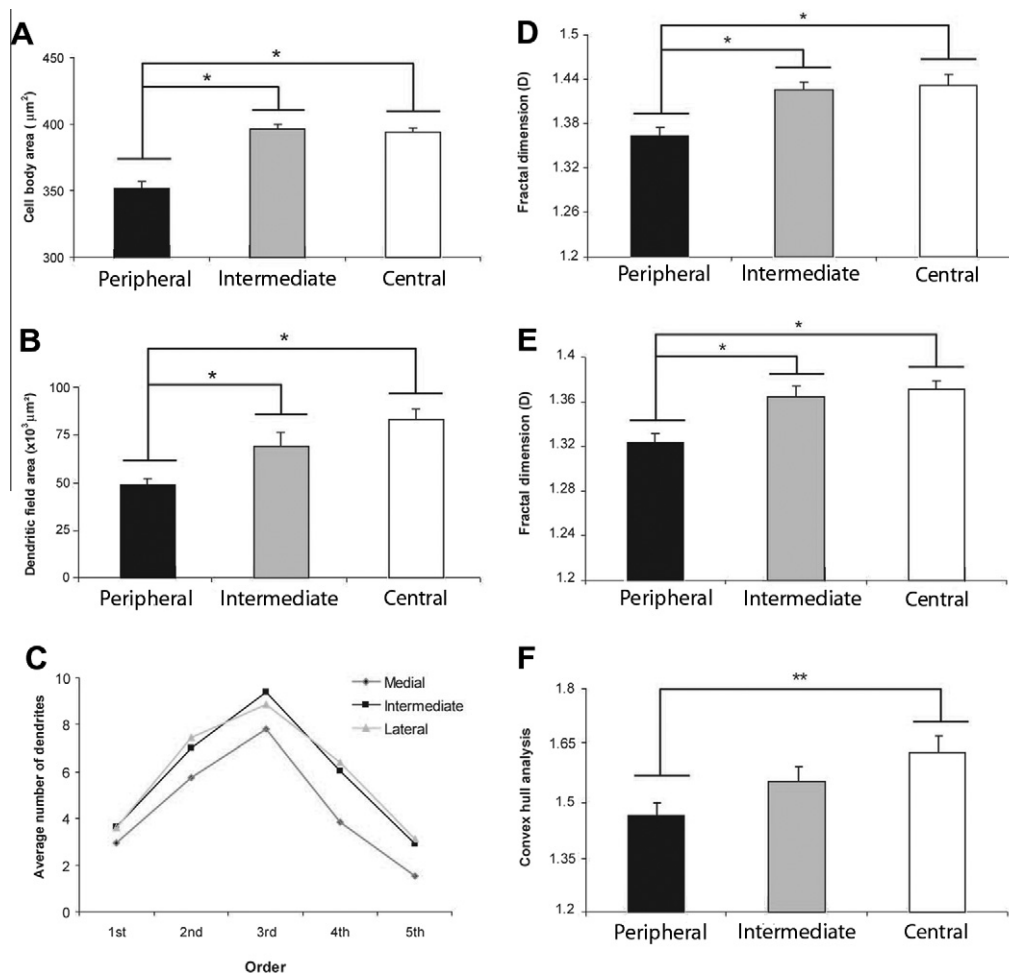


Fig. 3. Plots of the (A) cell body size, (B) dendritic field area, (C) number of dendritic branches by order, (D) mass radius fractal value, (E) dilatation fractal value and (F) convex hull analysis of NADPH-d type I neurons in the central, intermediate and peripheral visuotopic representation of agouti's V1. Neurons located in the central visuotopic representation are significantly larger than those found in the intermediate and peripheral representations ($*p < 0.05$) (A). The same trend was observed for dendritic field area (B), fractal dimension (mass radius – D; dilatation – E) and convex hull analysis (F) ($*p < 0.05$ and $**p < 0.01$, respectively). The highest number of dendritic branches occurred in the third order dendrites (C).

($F_{2,117} = 2.98$). *Post-hoc* pair-wise comparisons revealed a significant difference in cell body size between the populations of cells in the central and peripheral representa-

tions and between cells in the intermediate and peripheral representations, but not between cells in the central and intermediate representations ($p < 0.05$).

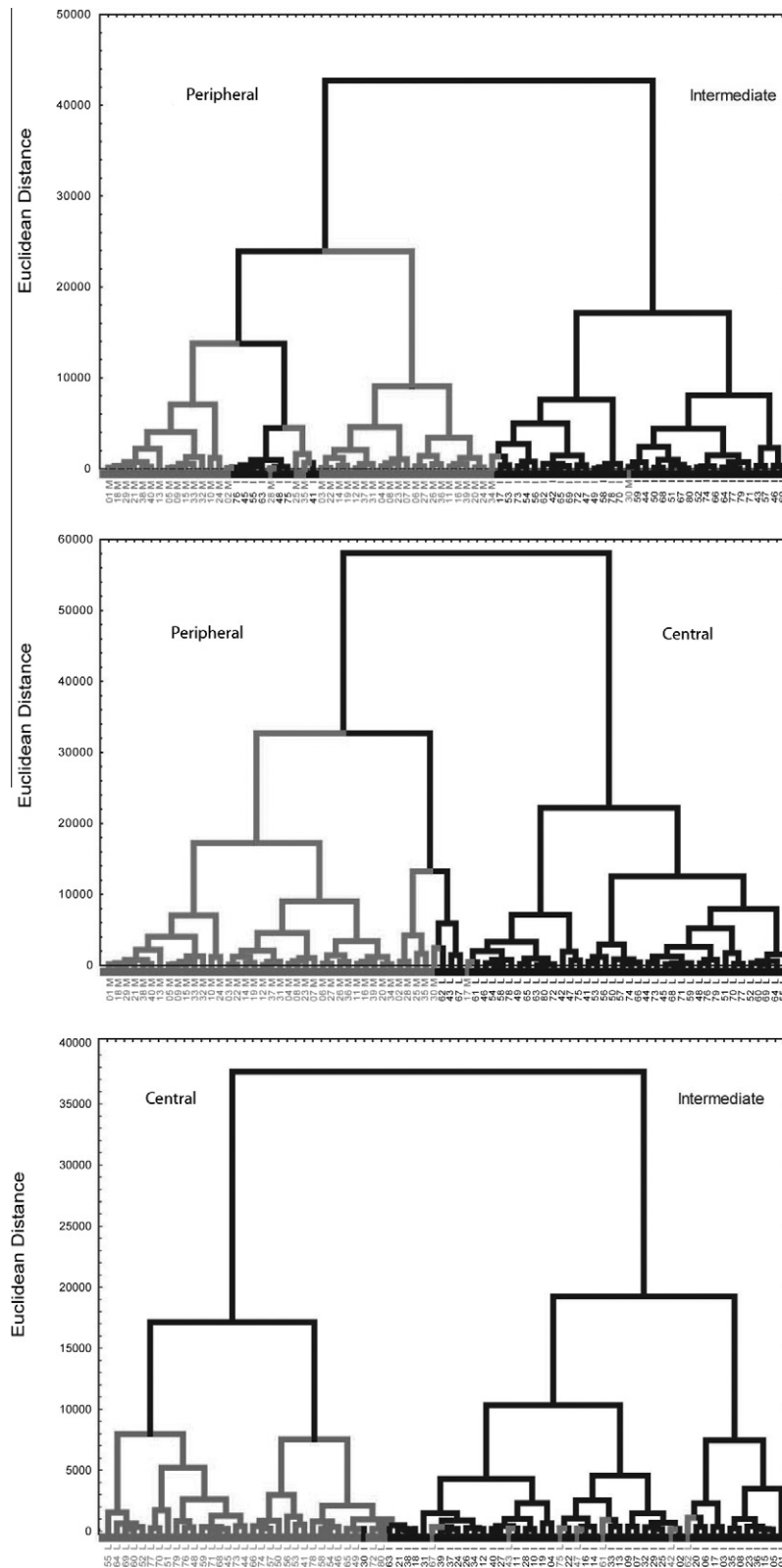


Fig. 4. Dendrograms revealed by cluster analysis of all neurons, with no *a priori* classification according to location within V1. Note the remarkable degree of separation of neurons according to the location within the visuotopic representation (central, intermediate and peripheral). Numbers at the bottom of each tree branch denote the identification number of the neuron.

The dendritic trees of NADPH-d type I neurons were largest in the central ($83.30 \pm 18.41 \times 10^3 \mu\text{m}^2$) representation, smaller in the intermediate representation ($68.28 \pm 17.41 \times 10^3 \mu\text{m}^2$) and smallest in the periphery ($47.89 \pm 12.35 \times 10^3 \mu\text{m}^2$) (Fig. 3B). An analysis of variance revealed these differences to be significant ($F_{2,117} = 6.27$). *Post-hoc* pair-wise comparisons revealed a significant difference in size of dendritic trees of neurons between the central and peripheral representations and between the intermediate and peripheral representations, but not between the central and intermediate representations ($p < 0.05$).

Analysis of the number of dendrites by order (Fig. 3C) revealed that neurons in the central and intermediate visuotopic representations of V1 were more branched than those in the peripheral representation, neurons in the former two regions having similar branching complexity. An analysis of variance revealed these differences to be significant ($F_{2,117} = 9.42$). *Post-hoc* pair-wise comparisons revealed a significant difference in the number of branches by order between cells in the peripheral representation, and those in the intermediate and central representations ($p < 0.05$). There was non-significant difference in the number of branches by order between neurons in the intermediate and central representations.

A similar finding was revealed by fractal analysis, by both the dilation (Fig. 3D) and mass radius (Fig. 3E) methods. Neurons in the central and intermediate visuotopic representations of V1 had higher fractal values (D) than those in the peripheral representations, neurons in the former two regions having similar D values: dilation (1.371 ± 0.009 , 1.365 ± 0.009 , 1.327 ± 0.008 , respectively), mass radius (1.437 ± 0.016 , 1.421 ± 0.015 , 1.365 ± 0.013 , respectively). An analysis of variance revealed these differences to be significant ($F_{2,117} = 3.74$). *Post-hoc* pair-wise comparisons revealed a significant difference in the D values of cells between the peripheral representation and the intermediate and central representations.

Convex hull analysis revealed that the dendritic trees of neurons in the central (1.655 ± 0.049) visuotopic representation were more 'complex' than those in the intermediate (1.571 ± 0.045) and peripheral (1.469 ± 0.037) representations (Fig. 3F). An analysis of variance revealed these differences to be significant ($F_{2,117} = 5.53$). *Post-hoc* pair-wise comparisons revealed a significant difference in the convex hull factor of cells in the peripheral and central representations.

Cluster analysis of neuronal morphology

In addition to testing morphological parameters of neurons according to their location within the visuotopic map within V1, we pooled all data and performed a cluster analysis of their morphological parameters. This analysis revealed striking separation of the neurons according to their eccentricity (Fig. 4). Three distinct clusters of neurons, each one containing neurons almost exclusively from either the central, intermediate or peripheral representations were identified. A discriminant analysis indicated that all morphological variables contributed to separation among these groups, including cell body size,

dendritic tree size, total length of dendrites, fractal dimension, and convex hull number.

DISCUSSION

In the present investigation we studied the morphology and distribution of NADPH-d-reactive neurons as a function of eccentricity along the naso-temporal representation in V1 of the agouti. We found: (1) NADPH-d histochemistry revealed the location and limits of V1, (2) the dendritic trees of NADPH-d type I neurons varied as a function of eccentricity, being larger and more branched in the central visuotopic representation compared with those in the peripheral representation, (3) the density of NADPH-d neurons differed as a function of eccentricity, being higher in the central visuotopic representation as compared with the peripheral representation.

The systematic nature of the variation in neuron structure reported here as a function of eccentricity makes us inclined to believe that the current results represent a cortical specialization, inconsistent with the notion of cortex being composed of a repeated 'canonical' circuit favored by some (Binzegger et al., 2005; Douglas and Martin, 2007; Heinze et al., 2007). Instead, we believe it more parsimonious that the present data reflect greater variation in circuit structure across the cortex than might be explained by normal variation in the 'ice-cube' model. Several additional lines of evidence support the view of regional specialization in circuitry, even within a cortical area. For example, systematic and significant differences have been reported in neuron density in V1 of primates (Collins et al., 2010), in patterns of connectivity of pyramidal cells and inhibitory interneurons in different barrel representations in rat's S1 (Elston et al., 1997, 1999a) and between pyramidal cells in mechanoreceptive *versus* electroreceptive cortex in S1 of the platypus (Elston et al., 1999b). Even greater differences in circuit structure have been reported when comparing neuron density and pyramidal cell structure and interneuron connectivity among cortical areas (Defelipe et al., 1999); (Elston et al., 1999b; Jacobs et al., 2001; Collins et al., 2010; Freire et al., 2012), which reportedly endow circuits with different functional capacity and behavioral outcomes (Jacobs et al., 2001; Elston, 2002, 2007; Spruston, 2008; Collins, 2011). Further systematic investigations in diverse cortical areas in more species are required to provide more clarity to the debate.

Interestingly, the NADPH-d-reactive neurons with the larger, more branched dendritic trees were located in the region of V1 characterized by a relatively high density of these cells, whereas the neurons with the smallest, least-branched dendritic trees were observed in cortex with a relatively low density of these cells. This finding is somewhat counterintuitive to the popular notion of a correlation between neuron density and dendritic tree structure. Moreover, Collins and colleagues (Collins et al., 2010) reported the reverse finding in V1 of primates: neuron density was higher in the central visuotopic representation than in the peripheral representation. However, these authors quantified the density of all neurons, whereas we quantified the density of a subset of inhibitory neurons.

It will be interesting to determine whether or not there may be opposite trends in neuron density as a function of eccentricity among inhibitory and excitatory neurons.

It is worth noting that our finding of a correlation between dendritic tree structure and eccentricity in V1 reflect observations made in subcortical visual centers such as the retina and the lateral geniculate nucleus (LGN; (Humphrey et al., 1985; Sur et al., 1987; Dacey, 1994); (Wright et al., 1997; Hendry and Reid, 2000; Dacey et al., 2003; Silveira et al., 2004; Poznanski, 2005; Field and Chichilnisky, 2007). However, in both the retina and the LGN the dendritic trees of neurons become increasingly larger from the central visuotopic representation to the peripheral representation. Further investigation will reveal whether or not other neuronal types, such as pyramidal cells, also differ systematically in the dendritic structure as a function of eccentricity in V1, and whether any such differences parallel those reported here.

Methodological limitations

As previously pointed out (Freire et al., 2012), there are several methodological limitations related to flattening cortical surface, tissue shrinkage and other structural modifications introduced by tissue processing. A flattened cortex potentially takes advantage of the two-dimensional topology of the cortical surface giving a global view of the cortical areas of interest in one single section. However due to the flattening procedure the possibility of metric distortions and altered results is important and these difficulties are difficult to overcome. On the other hand it is worth to note that in lissencephalic brains morphological distortion associated with flattening seems to be minimal (Freire et al., 2012). On the other hand due to mechanical factors associated with the vibratome sectioning and further dehydration procedure, a non-uniform shrinkage in the z-axis of the sections is obtained (Hosseini-Sharifabad and Nyengaard, 2007). Thus, estimates of modifications in the x/y dimensions during tissue processing cannot be linearly extrapolated to the z dimension. These methodological constraints impose limitations that have to be taken into consideration when analyzing the present data. However, it is important to note that an indication of a severe shrinkage in z-axis is the curling of dendrites, signifying that individual processes did not shrink at the same rate as the slice in which they are located. This pattern was not observed in the reconstructed cells of our study.

Taken together ours and other findings appear to be inconsistent with the 'ice-cube' model of cortical organization (Hubel and Wiesel, 1977) and theories of canonical circuits (Douglas and Martin, 2004), and suggest that stereotypy and diversity in the neocortex may or may not coexist both in the same and in different regions of the brain in different species (Katzel et al., 2011).

AUTHOR CONTRIBUTIONS

CWPD, LCLS, EGR and MAMF conceived and designed the experiments; CWPD, LCLS and EGR performed the experiments; CWPD, EGR and MAMF analyzed the data; MAMF, CWPD and GNE designed and organized the illustrations; CWPD, AP and GNE contributed intellectual

input and reagents/materials/analysis tools; CWPD, MAMF, EGR, AP, LCLS and GNE wrote the paper.

DISCLOSURE/CONFLICT-OF-INTEREST STATEMENT

The authors declare that the research was conducted in the absence of any commercial or financial relationships that could be construed as a potential conflict of interest.

Acknowledgements—Supported by grants from the Brazilian National Research Council (CNPq), CAPES and FAPESPA – Brazil. CWPD was supported by IBNnet-FINEP. GNE was supported by the National Health and Medical Research Council of Australia, the McDonnell Foundation (USA), the Centre for Cognitive Neuroscience (Australia) and the Hear and Say Centre (Australia). CWPD, AP and LCLS are CNPq research fellows.

REFERENCES

- Binzegger T, Douglas RJ, Martin KA (2005) Axons in cat visual cortex are topologically self-similar. *Cereb Cortex* 15:152–165.
- Collins CE (2011) Variability in neuron densities across the cortical sheet in primates. *Brain Behav Evol* 78:37–50.
- Collins CE, Airey DC, Young NA, Leitch DB, Kaas JH (2010) Neuron densities vary across and within cortical areas in primates. *Proc Natl Acad Sci U S A* 107:15927–15932.
- Conde F, Lund JS, Lewis DA (1996) The hierarchical development of monkey visual cortical regions as revealed by the maturation of parvalbumin-immunoreactive neurons. *Brain Res Dev Brain Res* 96:261–276.
- Dacey DM (1994) Physiology, morphology and spatial densities of identified ganglion cell types in primate retina. *Ciba Found Symp* 184:12–28. discussion 28–34, 63–70.
- Dacey DM, Peterson BB, Robinson FR, Gamlin PD (2003) Fireworks in the primate retina: in vitro photodynamics reveals diverse LGN-projecting ganglion cell types. *Neuron* 37:15–27.
- Defelipe J, Gonzalez-Albo MC, Del Rio MR, Elston GN (1999) Distribution and patterns of connectivity of interneurons containing calbindin, calretinin, and parvalbumin in visual areas of the occipital and temporal lobes of the macaque monkey. *J Comp Neurol* 412:515–526.
- Douglas RJ, Martin KA (2004) Neuronal circuits of the neocortex. *Annu Rev Neurosci* 27:419–451.
- Douglas RJ, Martin KA (2007) Mapping the matrix: the ways of neocortex. *Neuron* 56:226–238.
- Elston G (2007) Specializations in pyramidal cell structure during primate evolution. In: *Evolution of nervous systems*, Vol. 4 (Kaas J, TM P, eds), pp 191–242. Oxford: Academic Press.
- Elston GN (2002) Cortical heterogeneity: implications for visual processing and polysensory integration. *J Neurocytol* 31:317–335.
- Elston GN, Rosa MG (1997) The occipitoparietal pathway of the macaque monkey: comparison of pyramidal cell morphology in layer III of functionally related cortical visual areas. *Cereb Cortex* 7:432–452.
- Elston GN, Rosa MG (1998) Morphological variation of layer III pyramidal neurones in the occipitotemporal pathway of the macaque monkey visual cortex. *Cereb Cortex* 8:278–294.
- Elston GN, DeFelipe J, Arellano JI, Gonziles-Albo MC, Rosa MG (1999) Variation in the spatial relationship between parvalbumin immunoreactive interneurons and pyramidal neurones in rat somatosensory cortex. *Neuroreport* 10:2975–2979.
- Elston GN, Elston A, Aurelio-Freire M, Gomes Leal W, Dias IA, Pereira Jr A, Silveira LC, Picanco Diniz CW (2006) Specialization of pyramidal cell structure in the visual areas V1, V2 and V3 of the South American rodent, *Dasyprocta prymnolopha*. *Brain Res* 1106:99–110.

- Elston GN, Manger PR, Pettigrew JD (1999) Morphology of pyramidal neurones in cytochrome oxidase modules of the S-I bill representation of the platypus. *Brain Behav Evol* 53:87–101.
- Elston GN, Pow DV, Calford MB (1997) Neuronal composition and morphology in layer IV of two vibrissal barrel subfields of rat cortex. *Cereb Cortex* 7:422–431.
- Espinoza SG, Thomas HC (1983) Retinotopic organization of striate and extrastriate visual cortex in the hooded rat. *Brain Res* 272:137–144.
- Faro LR, Araujo R, Araujo M, Do-Nascimento JL, Friedlander MJ, Picanco-Diniz CW (1995) Localization of NADPH-diaphorase activity in the human visual cortex. *Braz J Med Biol Res* 28:246–251.
- Field GD, Chichilnisky EJ (2007) Information processing in the primate retina: circuitry and coding. *Annu Rev Neurosci* 30:1–30.
- Freire MA, Faber J, Picanco-Diniz CW, Franca JG, Pereira A (2012) Morphometric variability of nicotinamide adenine dinucleotide phosphate diaphorase neurons in the primary sensory areas of the rat. *Neuroscience* 205:140–153.
- Freire MA, Rocha EG, Oliveira JL, Guimaraes JS, Silveira LC, Elston GN, Pereira A, Picanco-Diniz CW (2010) Morphological variability of NADPH diaphorase neurons across areas V1, V2, and V3 of the common agouti. *Brain Res* 1318:52–63.
- Fujita I, Fujita T (1996) Intrinsic Connections in the macaque inferior temporal cortex. *J Comp Neurol* 368:467–486.
- Gabbott PL, Bacon SJ (1995) Co-localisation of NADPH diaphorase activity and GABA immunoreactivity in local circuit neurones in the medial prefrontal cortex (mPFC) of the rat. *Brain Res* 699:321–328.
- Gallyas F (1979) Silver staining of myelin by means of physical development. *Neurol Res* 1:203–209.
- Heinzle J, Hepp K, C Martin KA (2007) A microcircuit model of the frontal eye fields. *J Neurosci* 27:9341–9353.
- Hendry SH, Reid RC (2000) The koniocellular pathway in primate vision. *Annu Rev Neurosci* 23:127–153.
- Higo S, Udaka N, Tamamaki N (2007) Long-range GABAergic projection neurons in the cat neocortex. *J Comp Neurol* 503:421–431.
- Hosseini-Sharifabad M, Nyengaard JR (2007) Design-based estimation of neuronal number and individual neuronal volume in the rat hippocampus. *J Neurosci Methods* 162:206–214.
- Hubel DH, Wiesel TN (1974) Sequence regularity and geometry of orientation columns in the monkey striate cortex. *J Comp Neurol* 158:267–293.
- Hubel DH, Wiesel TN (1977) Ferrier lecture. Functional architecture of macaque monkey visual cortex. In: *Proceedings of the Royal Society of London Series B, Containing papers of a Biological character* 198:1–59.
- Humphrey AL, Sur M, Uhlich DJ, Sherman SM (1985) Projection patterns of individual X- and Y-cell axons from the lateral geniculate nucleus to cortical area 17 in the cat. *J Comp Neurol* 233:159–189.
- Jacobs B, Schall M, Prather M, Kapler E, Driscoll L, Baca S, Jacobs J, Ford K, Wainwright M, Treml M (2001) Regional dendritic and spine variation in human cerebral cortex: a quantitative golgi study. *Cereb Cortex* 11:558–571.
- Jelinek HF, Fernandez E (1998) Neurons and fractals: how reliable and useful are calculations of fractal dimensions? *J Neurosci Methods* 81:9–18.
- Katzel D, Zemelman BV, Buetfering C, Wolfel M, Miesenbock G (2011) The columnar and laminar organization of inhibitory connections to neocortical excitatory cells. *Nat Neurosci* 14:100–107.
- Kritzer MF, Cowey A, Somogyi P (1992) Patterns of inter- and intralaminar GABAergic connections distinguish striate (V1) and extrastriate (V2, V4) visual cortices and their functionally specialized subdivisions in the rhesus monkey. *J Neurosci* 12:4545–4564.
- Lund JS, Yoshioka T, Levitt JB (1993) Comparison of intrinsic connectivity in different areas of macaque monkey cerebral cortex. *Cereb Cortex* 3:148–162.
- Luth HJ, Hedlich A, Hilbig H, Winkelmann E, Mayer B (1994) Morphological analyses of NADPH-diaphorase/nitric oxide synthase positive structures in human visual cortex. *J Neurocytol* 23:770–782.
- Mountcastle VB (1957) Modality and topographic properties of single neurons of cat's somatic sensory cortex. *J Neurophysiol* 20:408–434.
- Mountcastle VB (1997) The columnar organization of the neocortex. *Brain* 120(Pt 4):701–722.
- Picanoço-Diniz C, G. RE, C SL, GN E, E O (2011) Cortical representation of the horizon in V1 and peripheral scaling in mammals with lateral eyes. *Psychol Neurosci* 4:19–27.
- Picanoço-Diniz CW, Oliveira HLS, Silveira LCL, Oswaldocruz E (1989) The visual cortex of the agouti (*Dasyprocta aguti*) – architectonic subdivisions. *Braz J Med Biol Res* 22:121–138.
- Picanoço-Diniz CW, Silveira L, Oswaldocruz E (1992) A comparative survey of magnification factor in V1 and retinal ganglion cell topography of lateral-eyed mammals English. In: *The visual system from genesis to maturity*, (Lent R, ed), pp 187–198. Rio de Janeiro: ed. Boston, USA: Birkhäuser.
- Picanoço-Diniz CW, Silveira LC, de Carvalho MS, Oswaldocruz E (1991) Contralateral visual field representation in area 17 of the cerebral cortex of the agouti: a comparison between the cortical magnification factor and retinal ganglion cell distribution. *Neuroscience* 44:325–333.
- Pincus Z, Theriot JA (2007) Comparison of quantitative methods for cell-shape analysis. *J Microsc* 227:140–156.
- Poznanski RR (2005) Biophysical mechanisms and essential topography of directionally selective subunits in rabbit's retina. *J Integ Neurosci* 4:341–361.
- Rocha EG, Santiago LF, Freire MA, Gomes-Leal W, Dias IA, Lent R, Houzel JC, Franca JG, Pereira Jr A, Picanco-Diniz CW (2007) Callosal axon arbors in the limb representations of the somatosensory cortex (SI) in the agouti (*Dasyprocta prymnolopha*). *J Comp Neurol* 500:255–266.
- Santiago LF, Rocha EG, Freire MA, Dias IA, Lent R, Houzel JC, Picanco-Diniz CW, Pereira Jr A, Franca JG (2007) The organizational variability of the rodent somatosensory cortex. *Rev Neurosci* 18:283–294.
- Scherer-Singler U, Vincent SR, Kimura H, McGeer EG (1983) Demonstration of a unique population of neurons with NADPH-diaphorase histochemistry. *J Neurosci Methods* 9:229–234.
- Schweitzer L, Renehan WE (1997) The use of cluster analysis for cell typing. *Brain Res Protoc* 1:100–108.
- Silveira LC, Saito CA, Lee BB, Kremers J, da Silva Filho M, Kilavik BE, Yamada ES, Perry VH (2004) Morphology and physiology of primate M- and P-cells. *Prog Brain Res* 144:21–46.
- Silveira LCL, Picancodiniz CW, Oswaldocruz E (1989) Distribution and size of ganglion-cells in the retinae of large amazon rodents. *Vis Neurosci* 2:221–235.
- Spruston N (2008) Pyramidal neurons: dendritic structure and synaptic integration. *Nat Rev* 9:206–221.
- Sur M, Esguerra M, Garraghty PE, Kritzer MF, Sherman SM (1987) Morphology of physiologically identified retinogeniculate X- and Y-axons in the cat. *J Neurophysiol* 58:1–32.
- Ts'o DY, Zarella M, Burkitt G (2009) Whither the hypercolumn? *J Physiol* 587:2791–2805.
- Vincent SR, Kimura H (1992) Histochemical mapping of nitric oxide synthase in the rat brain. *Neuroscience* 46:755–784.
- Wagor E, Mangini NJ, Pearlman AL (1980) Retinotopic organization of striate and extrastriate visual cortex in the mouse. *J Comp Neurol* 193:187–202.
- Wright LL, Macqueen CL, Elston GN, Young HM, Pow DV, Vaney DI (1997) The DAPI-3 amacrine cells of the rabbit retina. *Vis Neurosci* 14:473–492.